J Biomol NMR (2016) 65:143–156
DOI 10.1007/s10858-016-0045-x

ARTICLE

Evaluating the influence of initial magnetization conditions on extracted exchange parameters in NMR relaxation experiments: applications to CPMG and CEST

Tairan Yuwen[1] · Ashok Sekhar[1] · Lewis E. Kay[1,2]

Received: 26 April 2016 / Accepted: 28 June 2016 / Published online: 29 July 2016

Abstract Transient excursions of native protein states to functionally relevant higher energy conformations often occur on the μs–ms timescale. NMR spectroscopy has emerged as an important tool to probe such processes using techniques such as Carr–Purcell–Meiboom–Gill (CPMG) relaxation dispersion and Chemical Exchange Saturation Transfer (CEST). The extraction of kinetic and structural parameters from these measurements is predicated upon mathematical modeling of the resulting relaxation profiles, which in turn relies on knowledge of the initial magnetization conditions at the start of the CPMG/CEST relaxation elements in these experiments. Most fitting programs simply assume initial magnetization conditions that are given by equilibrium populations, which may be incorrect in certain implementations of experiments. In this study we have quantified the systematic errors in extracted parameters that are generated from analyses of CPMG and CEST experiments using incorrect initial boundary conditions. We find that the errors in exchange rates (k_{ex}) and populations (p_E) are typically small (<10 %) and thus can be safely ignored in most cases. However, errors become larger and cannot be fully neglected (20–40 %) as k_{ex} falls near the lower limit of each method or when short CPMG/CEST relaxation elements are used in these experiments. The source of the errors can be rationalized and their magnitude given by a simple functional form. Despite the fact that errors tend to be small, it is recommended that the correct boundary conditions be implemented in fitting programs so as to obtain as robust estimates of exchange parameters as possible.

Keywords Conformational exchange · CPMG · CEST · Spin relaxation · Boundary conditions

Introduction

Conformational exchange is closely linked to many important biological processes, including enzyme catalysis (Boehr et al. 2006; Henzler-Wildman et al. 2007; Ishima et al. 2001; Palmer 2015; Rivalta et al. 2012), ligand binding (Korzhnev et al. 2009; Sugase et al. 2007), and protein folding (Korzhnev et al. 2010; Neudecker et al. 2012). The conformational rearrangements that are typically involved can be of a large scale so that the functional dynamics occur on millisecond (or slower) timescales (Palmer 2014). In the case of biological exchange the resulting conformational ensemble is often highly biased towards the ground state, with the remaining states recalcitrant to study by conventional biophysical approaches (Sekhar and Kay 2013). However, since these so called 'excited' states may play important roles in function, despite their low populations (Baldwin and Kay 2009; Karplus and Kuriyan 2005), it is of great interest to characterize their structural and motional properties.

NMR spectroscopy has emerged as a powerful tool for characterizing molecular dynamics on many different

Electronic supplementary material The online version of this article (doi:10.1007/s10858-016-0045-x) contains supplementary material, which is available to authorized users.

✉ Lewis E. Kay
kay@pound.med.utoronto.ca

[1] Departments of Molecular Genetics, Biochemistry and Chemistry, The University of Toronto, Toronto, ON M5S 1A8, Canada

[2] Program in Molecular Structure and Function, Hospital for Sick Children, 555 University Avenue, Toronto, ON M5G 1X8, Canada

timescales (Baldwin and Kay 2009; Mittermaier and Kay 2006, 2009). For the study of chemical exchange processes there are a number of different NMR approaches that can be exploited, depending on the exact timescale of the dynamics, including CPMG (Palmer et al. 2001; Wang et al. 2003) and $R_{1\rho}$ relaxation dispersion (Mangia et al. 2010; Palmer and Massi 2006; Traaseth et al. 2012), CEST (Vallurupalli et al. 2012) and magnetization-exchange spectroscopy (Farrow et al. 1994; Montelione and Wagner 1989). CPMG and $R_{1\rho}$ relaxation dispersion are commonly used for studying molecular dynamics on the μs–ms timescale, while slower processes are often quantified using CEST ($\sim$3 to $\sim$20 ms) or magnetization exchange ($\sim$50 ms to $\sim$1 s) experiments. As is the case with all relaxation experiments (Noggle and Schirmer 1971), the analysis of chemical exchange data must take into account the appropriate initial conditions of magnetization (referred to as boundary conditions in what follows) immediately prior to the pulse sequence element that records the exchange process. The exact nature of the experiment used thus becomes of importance and it is quite possible that boundary conditions will change for a given class of experiment simply based on how it is executed.

Herein we focus largely on CPMG and CEST pulse schemes that are amongst the most popular for studying sparsely populated states of biomolecules (Sekhar and Kay 2013). In the case of a two-site exchanging system, $G \underset{k_{EG}}{\overset{k_{GE}}{\rightleftarrows}} E$, where G and E correspond to highly populated ground and sparsely populated excited conformers, respectively, analysis of either CPMG or CEST data allows the extraction of global exchange parameters such as p_E (= $1 - p_G$), the fractional population of state E, and $k_{ex} = k_{GE} + k_{EG}$, as well as per-residue chemical shift differences between spins in states G and E, $\Delta\varpi_{EG}$ (ppm) (Palmer et al. 2001). It is often the case in the analysis of CEST profiles that $\Delta\varpi_{EG}$ values can be readily obtained simply by inspection (Vallurupalli et al. 2012). Our impression is that the majority of analyses of CPMG or CEST data simply assume equilibrium populations to describe the magnetization of spins in the ground (p_G) and excited (p_E) states immediately prior to the CPMG/CEST relaxation elements. This need not be the case in general and it is of interest, therefore, to examine the size of errors in the extracted exchange parameters that are introduced when incorrect boundary conditions are used. Our goal is to focus exclusively on the errors introduced via boundary conditions and not on other error sources, many of which have already been described in the literature. Previous studies, in particular for CPMG, have focused on the influence of differential relaxation between exchanging spins in the ground and excited states, effects of homonuclear scalar couplings, evolution during refocusing pulses, data analysis assuming 2-state or 3-state models (Baldwin and Kay 2013; Hansen et al. 2012; Ishima and Torchia 2003, 2005, 2006; Korzhnev et al. 2004; Kovrigin et al. 2006) or the influence of differential R_1 relaxation rates for exchanging spins in the ground and excited states in the case of CEST (Fawzi et al. 2011; Vallurupalli et al. 2012). Herein we show from simulation and experiment that in most cases the errors resulting from using incorrect boundary conditions tend to be small, less than 10 % of the correct value and thus can be safely ignored. However, they do increase, to approximately 20–40 % as k_{ex} falls to near the lower detection limit for the CPMG or CEST experiments. Finally, we also consider an additional class of experiment that is used to measure the rates of amide hydrogen exchange with water. In this case the detected protein is the sparse state since the concentration of water greatly exceeds that of the protein and the correct estimate of initial boundary conditions now becomes essential for obtaining accurate exchange rates.

Materials and methods

Sample preparation

^{15}N-labeled FF domain containing the L24A mutation (L24A FF), ^{15}N-hTRF1 with the K52C mutation and U-^{15}N, ^{13}C labeled 4E-BP2 were expressed and purified following previously described protocols (Korzhnev et al. 2010; Lukhele et al. 2013; Sekhar et al. 2015). The final samples were: (1) 0.9 mM L24A FF in 50 mM sodium acetate pH 5.7, 100 mM NaCl, 1 mM EDTA and 10 % D_2O, (2) 0.4 mM K52C hTRF1 in 50 mM MES pH 6.0, 1 mM TCEP and 10 % D_2O and (3) 0.25 mM 4E-BP2 in 50 mM sodium phosphate pH 6.5, 100 mM NaCl, 1 mM EDTA, 1 mM benzamidine and 10 % D_2O.

NMR spectroscopy

^{15}N CPMG experiments on ^{15}N-labeled L24A FF were carried out on 500 MHz and 800 MHz spectrometers equipped with room-temperature probes using the TROSY version of the ^{15}N CPMG pulse sequence (Vallurupalli et al. 2007). A constant-time relaxation delay (T_{relax}) of 30 ms was used and ν_{CPMG} was sampled up to 1000 Hz. In order to extract intensities as a function of ν_{CPMG}, peaks were fitted using the software package FuDA (http://pound.med.utoronto.ca/~flemming/fuda/). Effective transverse relaxation rates, $R_{2,eff}$, were calculated based on peak intensities according to the relation $R_{2,eff}(\nu_{CPMG}) = -\ln(I(\nu_{CPMG})/I_o)/T_{relax}$, where I_o is the peak intensity in a reference spectrum recorded without the relaxation delay T_{relax} (Mulder et al. 2001).

^{15}N CEST experiments were recorded on K52C hTRF1 using a 600 MHz spectrometer equipped with a cryogenically cooled probe using a pulse sequence described previously (Vallurupalli et al. 2012). Datasets were acquired using an exchange time of 250 ms and two different B_1 field strengths $\sim$17 and $\sim$34 Hz. In each case, a reference spectrum was also recorded without the exchange delay. CEST profiles were constructed as the ratio of peak intensities with (I) and without (I_o) the exchange delay, T_{Ex}, as a function of the offset of the weak B_1 field. ^{1}H $R_{1\rho}$ experiments that are similar to those described by Ishima et al. (1998) but where water magnetization was preserved in some cases were acquired on a 600 MHz spectrometer equipped with a room-temperature probe using a 6 kHz ^{1}H spin-lock field applied during the relaxation delay (T_{relax}). T_{relax} values up to 40 ms were sampled, and the decrease in peak intensity with T_{relax} was fitted using mono-exponential ($Ae^{-R\tau}$) or modified mono-exponential functional forms ($Ae^{-R\tau} + C$). Relaxation decay profiles for in-phase or anti-phase (with respect to the attached nitrogen spin) amide ^{1}H magnetization were measured by placing ^{1}H spin-lock periods either before or after the ^{15}N chemical shift evolution delay, t_1, respectively. $R_{1\rho}$ decay profiles were also obtained using a modified version of the pulse sequence with the ^{1}H spin-lock period before t_1, where an additional 90° water-selective pulse is applied prior to a purge gradient, that eliminates water magnetization.

CPMG and CEST data fitting

The fitting of CPMG and CEST data sets was carried out using the software package ChemEx (https://github.com/gbouvignies/chemex). In total 38 and 21 residues without significant peak overlap were selected for analysis in CPMG and CEST experiments on L24A FF and K52C hTRF1, respectively. In the fitting of CPMG data, p_E, k_{ex}, $\Delta\varpi_{GE}$ and intrinsic transverse relaxation rates, R_2, were treated as fitting parameters (Korzhnev et al. 2004), while CEST data were analyzed using p_E, k_{ex}, $\Delta\varpi_{GE}$, R_1 (intrinsic longitudinal relaxation rates) and R_2 as fitting parameters (Vallurupalli et al. 2012). In both cases it was assumed that intrinsic longitudinal and transverse relaxation rates for spins in each state are identical, $R_{1,E} = R_{1,G}$, $R_{2,E} = R_{2,G}$ and p_E and k_{ex} were fit globally using a two-state exchange model. In the case of CEST, B_1 field inhomogeneity was modeled as described previously (Vallurupalli et al. 2012). Briefly, B_1 field inhomogeneity was taken into account by performing ten calculations with different B_1 fields evenly spaced between $\pm 2\sigma$ around the mean, where σ is the standard deviation of the measured B_1 field distribution ($\sim$10 % of the field). All ten calculations were averaged using coefficients that assumed a Gaussian profile. In order to estimate errors in the fitted parameters a bootstrap analysis was used (Press et al. 1998) with N = 1000 repeats under the assumption of either equilibrium or non-equilibrium initial boundary conditions (see text). Each of the 1000 data sets was constructed by randomly selecting residues with replacement from the original set used in the global fit. The number of residues thus used was always the same as for the original data. Each of the 1000 data sets was independently fit to a two-state model of exchange as described above to obtain distributions for p_E and k_{ex}.

Numerical simulations

Numerical simulations of CPMG and CEST data sets were carried out using ChemEx, with input parameters (Larmor frequency, B_1 field strength and inhomogeneity, $\Delta\varpi_{GE}$) that are as close as possible to those used experimentally. For CEST data B_1 field inhomogeneity was modeled as described above. CPMG and CEST data sets were generated by using either 'equilibrium' initial boundary conditions (magnetization of ground and excited states of p_G and p_E, respectively, immediately prior to the CPMG/CEST relaxation elements) or 'non-equilibrium' conditions where p_E is set to 0. Simulations were carried out using a two-state exchange model with p_E values of 1, 5 or 10 %. Values of exchange rates and relaxation times of $400\ s^{-1} \le k_{ex} \le 1500\ s^{-1}$ and $20\ ms \le T_{relax} \le 50$ ms were used in simulations of CPMG profiles while for CEST, $50\ s^{-1} \le k_{ex} \le 400\ s^{-1}$ and $100\ ms \le T_{Ex} \le 450$ ms. The simulated CPMG or CEST profiles were globally fit using a two-state exchange model, assuming either equilibrium or non-equilibrium initial boundary conditions. Since random noise is not used in simulations of data sets accurate exchange parameters can always be obtained from fits so long as the simulation and fitting procedures are carried out using the same initial boundary conditions, while fitting errors always exist if the simulation and fitting are performed with different initial boundary conditions.

Results and discussion

The problem

As discussed in the Introduction the analysis of CPMG and CEST data generally assumes that immediately prior to the chemical exchange delay, used to quantify exchange in each class of experiment, the magnetization from states G and E are given by the equilibrium populations, *i.e.*, p_G and p_E, respectively. This is almost certainly incorrect since the

relaxation properties of the corresponding nuclei in states G and E are unlikely to be the same. For example, in the slow exchange limit ($k_{ex} \ll \Delta\omega_{GE}$) the exchange contributions to the transverse relaxation rates of spins in G and E are given by $p_E k_{ex}$ and $(1 - p_E)k_{ex}$, that can be very different. Since the chemical exchange period, denoted by T_{relax} or T_{Ex} for CPMG or CEST, respectively, in what follows, is typically placed after several INEPT transfer steps, the large difference in relaxation rates may cause one state (typically the excited state) to decay much faster than the other during coherence transfer steps, creating non-equilibrium initial conditions. These effects can be mitigated to a certain extent by including additional delay elements that place magnetization along the z-axis immediately before and after T_{relax} or T_{Ex} (Hansen et al. 2008), so that an equilibration can occur, although their efficiency depends on the exchange rate(s). Moreover, the initial state populations are not only a function of the (relaxation) properties of the spin system but also depend on how the measurement is performed, so that even assuming that the relaxation rates of spins in the ground and excited states are equivalent there can still be deviations in initial conditions from those expected for an 'equilibrium' spin system. For example, it is possible to design pulse schemes where the t_1 frequency-labeling period is placed either before or after the chemical exchange period. In the case of ^{15}N CPMG or ^{15}N CEST data sets recorded as HSQC-based experiments placement of the relaxation element prior to t_1 evolution allows the preservation of both cosine and sine modulated t_1 components of magnetization, leading to an improvement in spectral sensitivity by as much as a factor of $\sqrt{2}$ (Kay et al. 1992; Palmer et al. 1991; Schleucher et al. 1993). In contrast, Ishima et al. argue that it is important to record amide ^{1}H CPMG experiments by using a scheme that places the t_1 element before the CPMG interval so as to minimize the effects of homonuclear ^{1}H cross-relaxation (Ishima et al. 1998) that varies as a function of CPMG pulsing frequency. Thus, in this scheme magnetization from states G and E is modulated by terms such as $\cos(\omega_N^G t_1)$ and $\cos(\omega_N^E t_1)$, respectively, prior to T_{relax} that effectively sets the initial magnetization of state E to 0. This can be readily understood by noting that magnetization that originates on state E and subsequently transferred to state G via exchange leads to a cross peak at (ω_N^E, ω_H^G) that is distinct from the corresponding cross peak position of the major state (ω_N^G, ω_H^G), assuming $\omega_N^E \neq \omega_N^G$. Since the major state cross peak is quantified in these experiments the initial state is effectively $(M_G, M_E) = (p_G, 0)$, where M_G and M_E are the relevant magnetization elements (either transverse for CPMG, or longitudinal for CEST). By contrast, in experiments where the relaxation element precedes t_1 evolution, the initial magnetization from *both* states E and G contributes to the observed signal (state G, see below) and the initial conditions are $(M_G, M_E) = (p_G, p_E)$, assuming (often incorrectly) similar relaxation losses for both states during the delays in the pulse scheme. We will refer to the situation, where the effective initial magnetization is $(p_G, 0)$, as the "non-equilibrium" case and where it is (p_G, p_E) as the "equilibrium" case in what follows. The errors in the exchange parameters that are introduced by the use of incorrect initial magnetization conditions in data fitting routines will be discussed below.

Dependence of relaxation rates on the initial conditions for systems in two-site exchange

In what follows we first consider the CPMG experiment and focus, therefore, on the evolution of transverse magnetization, $M_{G,+}$ and $M_{E,+}$, from the ground and excited states, respectively. In the free precession limit the evolution of the exchanging magnetization can be simply described by the Bloch–McConnell equations (McConnell 1958)

$$\begin{aligned} \frac{dM_{G,+}}{dt} &= -\left(R_{2,G} + k_{GE}\right)M_{G,+} + k_{EG}M_{E,+}, \\ \frac{dM_{E,+}}{dt} &= k_{GE}M_{G,+} - \left(R_{2,E} + k_{EG} - i\Delta\omega_{GE}\right)M_{E,+} \end{aligned} \quad (1)$$

where $R_{2,G}$ and $R_{2,E}$ are the intrinsic transverse relaxation rates for magnetization in states G and E, respectively. In the limit that $p_G \gg p_E$ considered here, only magnetization from the ground state is observable (in both CPMG and CEST experiments), so that the following discussion will focus only on $M_{G,+}$ for different initial conditions. For simplicity, it is assumed that the final detected signal intensity is proportional to the magnitude of ground state magnetization at the end of the exchange duration. Here we do not take into account additional elements in the pulse sequence (e.g., t_1 or INEPT elements) that may alter the relative intensities of magnetization from the ground and excited states, but this is not necessary for the conclusions we wish to make.

Inspection of Eq 1 shows that in the slow exchange regime ($k_{ex} \ll \Delta\omega_{GE}$) the transverse relaxation of the ground state, $R_{2,eff}$, is increased by $k_{GE} = p_E k_{ex}$ and that the decay of ground state magnetization is independent of the excited state magnetization. In general, however, the decay of both $M_{G,+}$ and $M_{E,+}$ are coupled, leading to bi-exponential relaxation (Hansen and Led 2003; McConnell 1958). In the limiting case where $\Delta\omega_{GE} \to 0$, corresponding to very rapid pulsing in the CPMG experiment, $\nu_{CPMG} \to \infty$ (where $\nu_{CPMG} = 1/(2\delta)$ and δ is the spacing between successive refocusing pulses) the Bloch–McConnell equations can be written as

$$\frac{dM_{G,+}}{dt} = -\left(R_{2,G} + k_{GE}\right)M_{G,+} + k_{EG}M_{E,+},$$
$$\frac{dM_{E,+}}{dt} = k_{GE}M_{G,+} - \left(R_{2,E} + k_{EG}\right)M_{E,+}. \quad (2)$$

The general solution to these equations is (with $M^{\infty}_{G,+} = M^{\infty}_{E,+} = 0$):

$$M_{G,+}(\tau) = \Lambda_1 e^{\lambda_1\tau} + \Lambda_2 e^{\lambda_2\tau},$$
$$M_{E,+}(\tau) = \Lambda_3 e^{\lambda_1\tau} + \Lambda_4 e^{\lambda_2\tau} \quad (3)$$

where

$$\lambda_{1,2} = \frac{-(R_{2,G} + R_{2,E} + k_{ex}) \pm \sqrt{(-R_{2,G} + R_{2,E} + k_{ex})^2 + 4p_E(R_{2,G} - R_{2,E})k_{ex}}}{2} \quad (4)$$

and

$$\Lambda_1 = \frac{-(\lambda_2 + R_{2,G} + k_{GE})M_{G,+}(0) + k_{EG}M_{E,+}(0)}{\lambda_1 - \lambda_2},$$
$$\Lambda_2 = \frac{(\lambda_1 + R_{2,G} + k_{GE})M_{G,+}(0) - k_{EG}M_{E,+}(0)}{\lambda_1 - \lambda_2},$$
$$\Lambda_3 = \frac{k_{GE}M_{G,+}(0) + (\lambda_1 + R_{2,G} + k_{GE})M_{E,+}(0)}{\lambda_1 - \lambda_2},$$
$$\Lambda_4 = \frac{-k_{GE}M_{G,+}(0) - (\lambda_2 + R_{2,G} + k_{GE})M_{E,+}(0)}{\lambda_1 - \lambda_2}. \quad (5)$$

Assuming that $\left|R_{2,G} - R_{2,E}\right| \ll k_{ex}$ the eigenvalues of the relaxation matrix become

$$\lambda_1 = -[(1 - p_E)R_{2,G} + p_E R_{2,E}],$$
$$\lambda_2 = -[(1 - p_E)R_{2,E} + p_E R_{2,G} + k_{ex}] \quad (6)$$

and the coefficients for the bi-exponential decay are

$$\Lambda_1 = \frac{[(1-p_E)(R_{2,E} - R_{2,G}) + k_{EG}]M_{G,+}(0) + k_{EG}M_{E,+}(0)}{(1-2p_E)(R_{2,E} - R_{2,G}) + k_{ex}},$$
$$\Lambda_2 = \frac{[p_E(R_{2,G} - R_{2,E}) + k_{GE}]M_{G,+}(0) - k_{EG}M_{E,+}(0)}{(1-2p_E)(R_{2,E} - R_{2,G}) + k_{ex}},$$
$$\Lambda_3 = \frac{k_{GE}M_{G,+}(0) + [p_E(R_{2,G} - R_{2,E}) + k_{GE}]M_{E,+}(0)}{(1-2p_E)(R_{2,E} - R_{2,G}) + k_{ex}},$$
$$\Lambda_4 = \frac{-k_{GE}M_{G,+}(0) + [(1-p_E)(R_{2,E} - R_{2,G}) + k_{EG}]M_{E,+}(0)}{(1-2p_E)(R_{2,E} - R_{2,G}) + k_{ex}}. \quad (7)$$

A similar set of equations applies when both ground and excited state magnetization are aligned along the z-axis, with M_+ and R_2 replaced by M_z and R_1. This assumes that the phase cycle eliminates contributions from equilibrium longitudinal magnetization, as is commonly the case experimentally (Sklenar et al. 1987; Vallurupalli et al. 2012). Equations 2–7 are thus germane for CEST experiments in the case where the weak B_1 field is not applied near resonance frequencies of the ground or excited state spins.

Errors caused by using incorrect initial conditions in fits of CPMG dispersion profiles

In order to first establish how boundary conditions influence the resultant dispersion profiles we have simulated curves for a single residue obtained with initial conditions of either $(M_{G,+}(0), M_{E,+}(0)) = (p_G M^o_+, p_E M^o_+)$ ('equilibrium' case) or $(M_{G,+}(0), M_{E,+}(0)) = (p_G M^o_+, 0)$ ('non-equilibrium' case). In panel a of Fig. 1 $\Delta\varpi_{GE} = 5$ ppm, so that the chemical shift exchange timescale is in the slow regime for $\nu_{CPMG} = 0$ ($k_{ex}/\Delta\omega_{GE} \simeq 0.3$). The simulation was carried out assuming that $R_2 = 0$ s^{-1} for spins in both states, noting that $R_2 > 0$ s^{-1} only causes a systematic shift to the dispersion profiles without changing the overall shape. In the slow pulsing limit the system remains in slow exchange and the decay profile of ground state magnetization $M_{G,+}$ is independent of the initial value of $M_{E,+}(0)$, as described above (inset a in Fig. 1a). As CPMG pulses are applied more frequently the effective shift difference between spins in states G and E decreases so that the system is driven into the fast exchange regime. Equations 2–7 establish that in the rapid pulsing limit the decay of the ground state magnetization depends on $M_{E,+}(0)$ (insets b, c). Thus, differences in profiles are expected for equilibrium and non-equilibrium conditions (Fig. 1a, blue *vs* red curves). In particular, the different initial magnetization conditions lead to a systematic shift in the plateau of the CPMG dispersion profile, and the magnitude of such a shift can be quantitatively evaluated based on equations of the previous section. In the 'equilibrium case', $k_{GE}M_{G,+}(0) = k_{EG}M_{E,+}(0)$, and for $\nu_{CPMG} \to \infty$, the decay of $M_{G,+}$ is mono-exponential, and given to good approximation by $M_{G,+}(\tau) = e^{-[(1-p_E)R_{2,G} + p_E R_{2,E}]\tau}M_{G,+}(0)$ (assuming $\left|R_{2,G} - R_{2,E}\right| \ll k_{ex}$). In contrast, in the 'non-equilibrium' case where $M_{E,+}(0) = 0$ (CPMG element after t_1 evolution) the decay of $M_{G,+}$ is bi-exponential

$$M_{G,+}(\tau) = \left[\begin{array}{l} \frac{(1-p_E)(R_{2,E} - R_{2,G} + k_{ex})}{(1-2p_E)(R_{2,E} - R_{2,G}) + k_{ex}} e^{-[(1-p_E)R_{2,G} + p_E R_{2,E}]\tau} \\ + \frac{p_E(R_{2,G} - R_{2,E} + k_{ex})}{(1-2p_E)(R_{2,E} - R_{2,G}) + k_{ex}} e^{-[(1-p_E)R_{2,E} + p_E R_{2,G} + k_{ex}]\tau} \end{array}\right] M_{G,+}(0) \quad (8)$$

and the relative weights of the slow and fast decaying components are well approximated by $1 - p_E$ and p_E respectively. For typical values of T_{relax} used in most CPMG experiments (20–50 ms) the fast decaying component vanishes during T_{relax} and the decay of $M_{G,+}$ becomes single exponential, $M_{G,+}(\tau) \approx (1 - p_E)e^{-[(1-p_E)R_{2,G} + p_E R_{2,E}]\tau}M_{G,+}(0) = e^{-[(1-p_E)R_{2,G} + p_E R_{2,E} - \ln(1-p_E)/\tau]\tau}M_{G,+}(0)$. Thus the

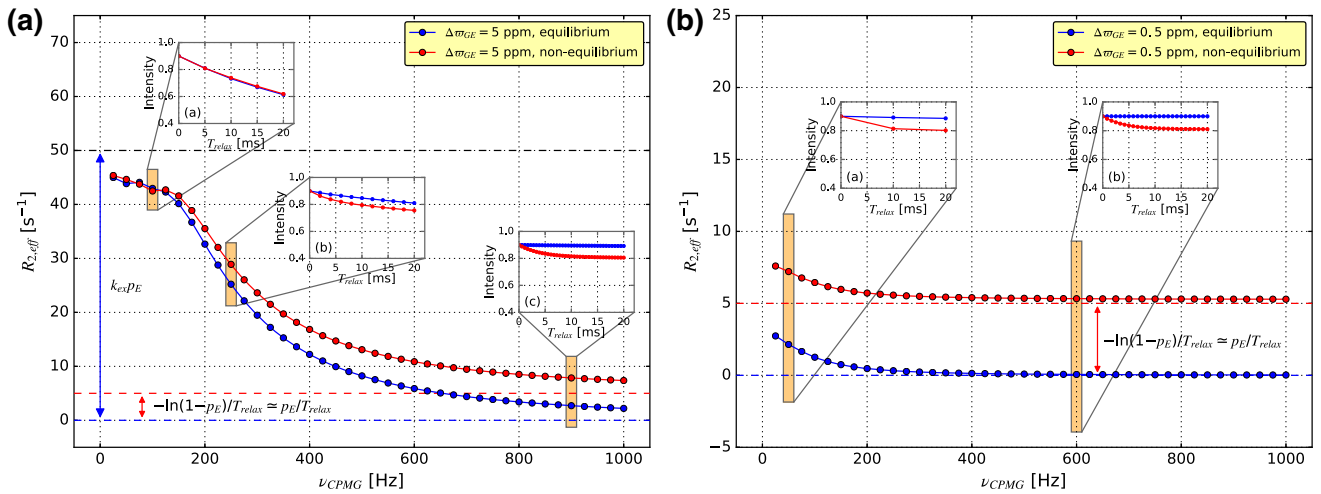

Fig. 1 Simulated ^{15}N CPMG relaxation dispersion profiles (500 MHz) for a single residue undergoing two-site chemical exchange. The following parameters were used: $T_{relax} = 20$ ms, $p_E = 0.10$, $k_{ex} = 500$ s^{-1}. Dispersion curves in **a** and **b** were simulated with $\Delta\varpi_{GE} = 5$ ppm and $\Delta\varpi_{GE} = 0.5$ ppm respectively, using 'equilibrium' (*blue*) or 'non-equilibrium' (*red*) initial conditions and assuming that $R_{2,G} = R_{2,E} = 0$ s^{-1}. The *insets in each panel* display magnetization decay profiles as a function of T_{relax} for different ν_{CPMG} values, with the magnitude of M_G sampled only at the end of each CPMG pulse element (δ/2 – 180° – δ/2)

$R_{2,eff}(\nu_{CPMG} = \infty)$ values for 'equilibrium' and 'non-equilibrium' cases will differ by $-\ln(1 - p_E)/T_{relax} \simeq p_E/T_{relax}$, corresponding to the magnitude of the shift in plateau positions between the CPMG dispersion profiles that are illustrated in Fig. 1.

For exchanging spins where $\Delta\varpi_{GE}$ is much smaller (Fig. 1b, $\Delta\varpi_{GE} = 0.5$ ppm, $k_{ex}/\Delta\omega_{GE} \simeq 3$) the system is always in the fast exchange regime so that the 'equilibrium' and 'non-equilibrium' profiles are shifted by an identical amount for all ν_{CPMG} values. In this case the same exchange parameters will be obtained from fits using either of the two boundary conditions. The two examples of Fig. 1, corresponding to cases of slow and fast exchange in the absence of pulsing, were chosen as extreme examples to illustrate in an intuitive manner the range of errors that could be expected when using incorrect initial magnetization conditions. In practice, the analysis of CPMG data is carried out by a global fitting of multiple residues that generally span a range of exchange regimes (Korzhnev et al. 2004). Errors in fitting parameters would thus be expected, in general, if the boundary conditions used are incorrect.

In order to appreciate the magnitude of the errors involved in what follows we consider the case where CPMG relaxation dispersion profiles are recorded with the t_1 evolution period preceding the CPMG interval, $t_1 - (\delta/2 - 180° - \delta - 180° - \delta/2)_n$, as for the amide ^{1}H CPMG scheme of Ishima et al. (1999). In this case the initial conditions become $M_{G,+}(0) = p_G M_+ \cos(\omega_N^E t_1)$, $M_{E,+}(0) = p_E M_+ \cos(\omega_N^E t_1)$, neglecting the effects of relaxation during the course of the delays in the pulse scheme. Because the contribution from $M_{E,+}(0)$ is modulated by ω_N^E and not ω_N^G during t_1, while the CPMG profile is derived from the intensity of the cross peak at (ω_N^G, ω_H^G) (ground state correlation) there is effectively no contribution from $M_{E,+}(0)$ to the resultant dispersion curve, so long as $\omega_N^E \neq \omega_N^G$. Thus, the appropriate boundary condition in fits of dispersion data in this case is $M_{E,+}(0) = 0$. We have numerically simulated ^{15}N CPMG profiles ($M_{E,+}(0) = 0$) for a range of exchange parameters (400 s^{-1} $\leq k_{ex} \leq$ 1500 s^{-1}, 20 ms $\leq T_{relax} \leq$ 50 ms) using 38 'residues' with $\Delta\varpi_{GE}$ values that are the same as those experimentally determined for the L24A FF domain that interconverts between folded (ground) and folding intermediate (excited) conformers (Korzhnev et al. 2010). Thus, a range of chemical shift exchange time-scales is represented in the complete data set, as would be the case in the analysis of experimental profiles (see below). Data were generated at a pair of B_o fields (11.7 and 18.7 T) and then globally fit to a two-site exchange model assuming that $M_{G,+}(0) = p_G M_+^o$ and $M_{E,+}(0) = p_E M_+^o$, as is frequently done using conventional programs. Output parameters were compared with the input values to estimate the errors arising from using incorrect initial conditions, Fig. 2, and the fitting errors are less than 10 % in most cases.

The magnitude of the fitting errors can be estimated in a qualitative and intuitive manner for the case where data sets recorded using 'non-equilibrium' initial conditions are analyzed using a model that assumes 'equilibrium' populations at the start of the CPMG interval, as was done here. Since the total size of the dispersion profile, corresponding to $R_{2,eff}(\nu_{CPMG} = 0) - R_{2,eff}(\nu_{CPMG} = \infty)$, is $p_E k_{ex}$ in the slow exchange limit and it is reduced by p_E/T_{relax} due to the upward

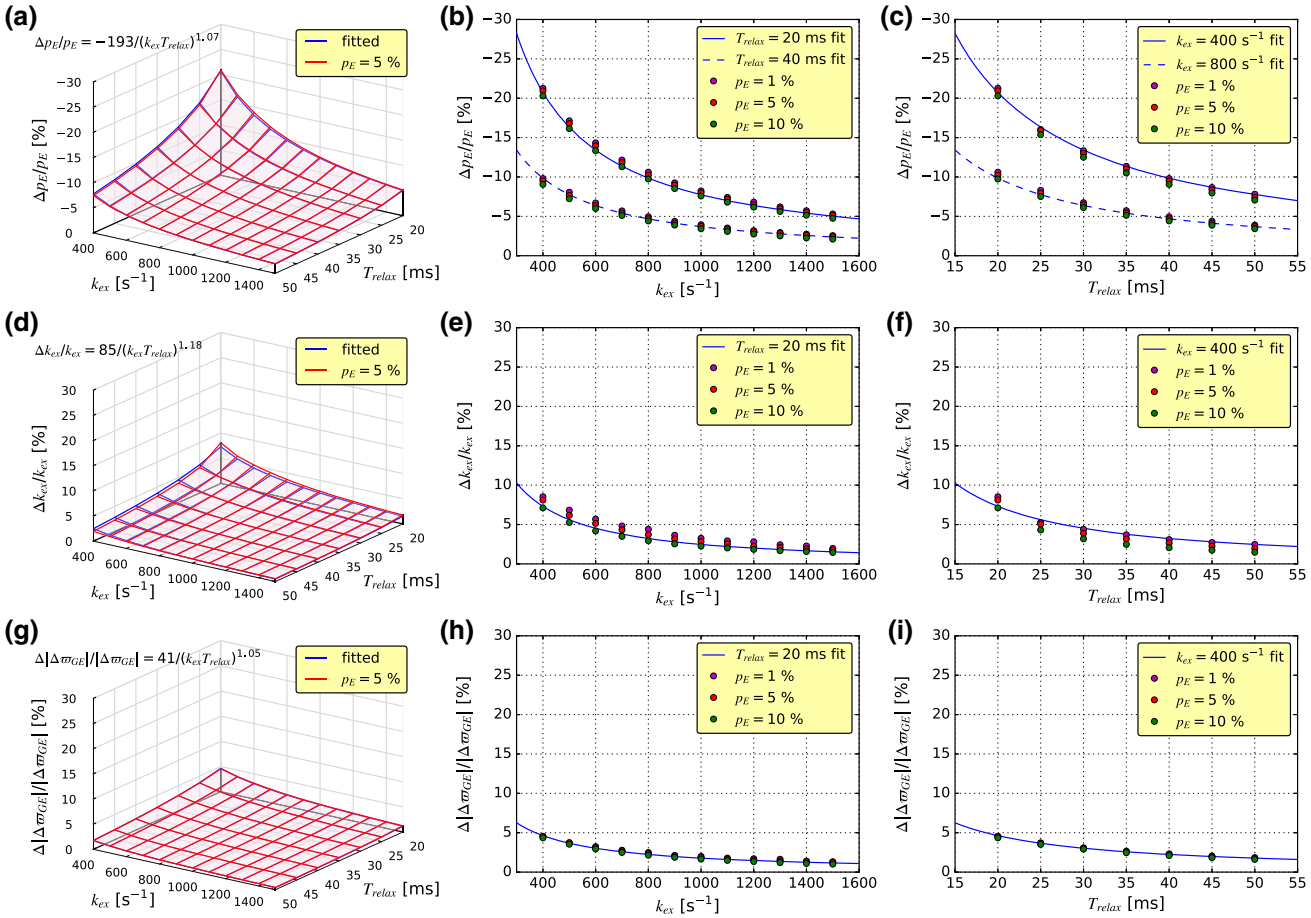

Fig. 2 Systematic errors in exchange parameters result from fits of ^{15}N CPMG profiles using incorrect initial boundary conditions. In all cases, 'non-equilibrium' initial conditions were used to generate simulated data that were then fit under the assumption of 'equilibrium' initial conditions. **a**–**c** Relative errors in p_E, **d**–**f** relative errors in k_{ex}, **g**–**i** relative errors in $\Delta\varpi_{GE}$. Errors in $\Delta\varpi_{GE}$ are obtained as averages over all the residues included in the global fit of the data. **a**, **d**, **g** The *red surface* is the one generated via simulation with $p_E = 5$ % and the *blue surface* is generated by fitting simulated data sets obtained with $p_E = 1$, 5, 10 % simultaneously and given by the equation in the *upper left hand corners*. In the remaining *panels* the *dashed and solid lines* are generated with the fitted equation for the error surface. Two sets of simulated fitting errors with different T_{relax} or k_{ex} are displayed in **b** and **c**. $\Delta R_2 = 0$ s^{-1}

shift of the plateau in the 'non-equilibrium' case it might be expected that the relative fitting error would be related to $(p_E/T_{relax})/(p_E k_{ex})$, that is proportional to $1/(k_{ex}T_{relax})$. Figure 2 plots relative fitting errors as a function of exchange parameters p_E, k_{ex} and T_{relax}. As expected, relative fitting errors show little dependence on p_E but are closely related to k_{ex} and T_{relax}, and can be well characterized using a simple functional form $A/(k_{ex}T_{relax})^c$. Notably, p_E values tend to be smaller and k_{ex} larger than the input parameters, with the decrease in p_E larger than the increase in k_{ex}, such that the product $p_E k_{ex}$ is smaller than the input. Although fitting errors are small (<10 %) in most cases, relatively large errors are observed for short T_{relax} values and as k_{ex} approaches the lower limit for the CPMG experiment, for example errors on the order of 20 % in p_E for $k_{ex} = 400$ s^{-1} and $T_{relax} = 20$ ms.

We have also repeated the calculations for a number of cases where ground and excited state spins have different intrinsic relaxation rates, $\Delta R_2 = R_{2,E} - R_{2,G}$, Figures S1–S3. The fitting errors are similar for different values of ΔR_2 over the range of k_{ex} and T_{relax} that have been simulated with the values of A and c that describe the error curve, $A/(k_{ex}T_{relax})^c$, listed in Table 1. Notably, errors increase as ΔR_2 grows. This can be understood by noting that the relative fitting error now becomes $\sim(p_E/T_{relax})/(p_E k_{ex} - p_E\Delta R_2)$ since the size of the dispersion decreases by $p_E\Delta R_2$. A similar analysis to that given above but assuming 'equilibrium' initial conditions and fitting with 'non-equilibrium' magnetization values (Figure S4, Table S1) also establishes that small errors in exchange parameters are obtained.

Table 1 The pre-factor A and the exponential factor c, for the equation $A/(k_{ex}T_{relax})^c$ describing the relative errors in fitting parameters when CPMG profiles generated with 'non-equilibrium' boundary conditions are fit using equilibrium initial values of magnetization

	$\Delta R_2 = 0\ s^{-1}$		$\Delta R_2 = 20\ s^{-1}$		$\Delta R_2 = 200\ s^{-1}$	
	A	c	A	c	A	c
p_E	−193	1.07	−201	1.08	−253	1.12
k_{ex}	85	1.18	96	1.21	161	1.31
$\Delta\varpi_{GE}$	41	1.05	42	1.05	37	1.00

Errors caused by using incorrect initial conditions in fits of CEST profiles

Prior to discussing the errors that derive from 'incorrect' fits of CEST data we first illustrate the dependence of CEST profiles on initial magnetization conditions by considering a single residue, Fig. 3, as was done above in the analysis of CPMG profiles. The most obvious consequence of the different initial conditions is the baseline shift in the CEST profiles. When the weak B_1 field is not applied near the resonance positions of spins in the ground and excited states, magnetization for states G and E is aligned along the z-axis and the exchange regime is analogous to that of fast interconversion discussed above for the CPMG experiment in the limit where $\nu_{CPMG} \rightarrow \infty$. In the case where the initial magnetization conditions are $(M_{G,z}(0), M_{E,z}(0)) = (p_G M_z^o, 0)$, the magnetization that is effectively lost from state G is not replenished through exchange with E, so that the intensity of the signal from G (I in Fig. 3, where I_o is the corresponding intensity for $T_{Ex} = 0\ s^{-1}$) is reduced relative to the 'equilibrium' case. This can also be seen mathematically using equations analogous to those for the CPMG experiment. For example, in the case where $(M_{G,z}(0), M_{E,z}(0)) = (p_G M_z^o, p_E M_z^o)$, the decay of the ground state longitudinal magnetization is, to an excellent approximation, mono-exponential $M_{G,z}(\tau) = e^{-[(1-p_E)R_{1,G}+p_E R_{1,E}]\tau} M_{G,z}(0)$ (assuming that $|R_{1,G} - R_{1,E}| \ll k_{ex}$), while for $M_{E,z}(0) = 0$ the decay is bi-exponential (see Eq. (7))

$$M_{G,z}(\tau) = \left[\begin{array}{l} \dfrac{(1-p_E)(R_{1,E}-R_{1,G}+k_{ex})}{(1-2p_E)(R_{1,E}-R_{1,G})+k_{ex}} e^{-[(1-p_E)R_{1,G}+p_E R_{1,E}]\tau} \\ + \dfrac{p_E(R_{1,G}-R_{1,E}+k_{ex})}{(1-2p_E)(R_{1,E}-R_{1,G})+k_{ex}} e^{-[(1-p_E)R_{1,E}+p_E R_{1,G}+k_{ex}]\tau} \end{array} \right] M_{G,z}(0) \quad (9)$$

where the relative weights of the slow and fast decaying components are $1 - p_E$ and p_E, respectively. For typical values of k_{ex} and T_{Ex} the fast decaying component should vanish nearly completely and the magnitude of the baseline shift in CEST profiles generated with 'equilibrium' and 'non-equilibrium' initial conditions becomes $p_E e^{-[(1-p_E)R_{1,G}+p_E R_{1,E}]T_{Ex}}$.

The relative I/I_o values for the dips in Fig. 3 can also be simply understood. When the weak B_1 field (x-axis) is applied near the resonance frequency of the exchanging spin in the excited state, M_E precesses about the x-axis and if the rate of precession is fast compared to k_{ex} net magnetization is not transferred from E to G, independent of the initial boundary conditions, analogous to the slow exchange condition in the CPMG experiment. A similar situation holds in the case where the B_1 field is applied on resonance with the ground state spin. Thus, I/I_o values are expected to be essentially independent of initial conditions for both dips in the CEST profile, as observed in Fig. 3.

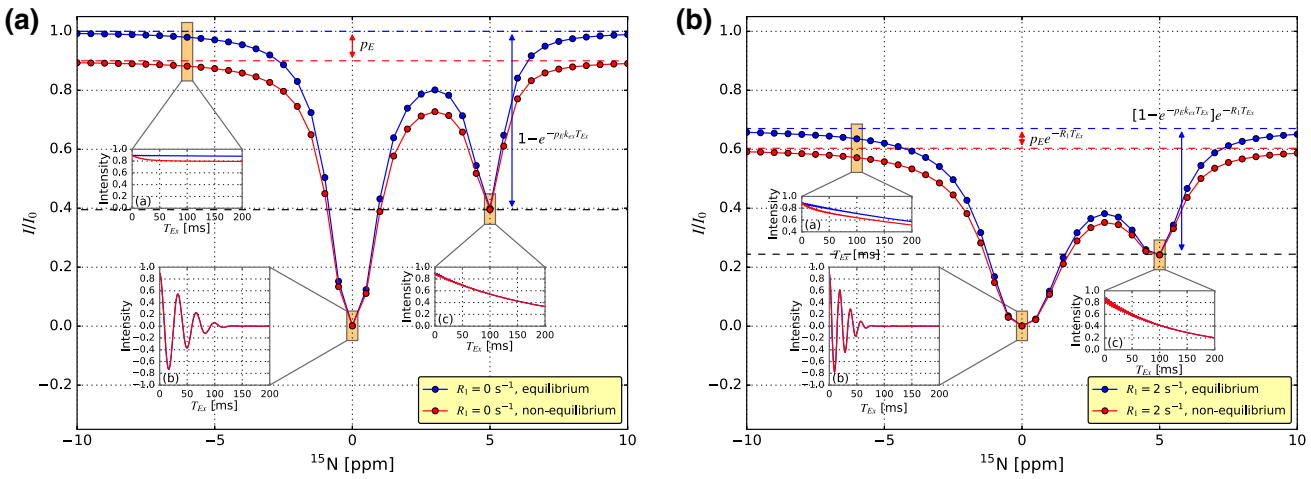

Fig. 3 ^{15}N CEST profiles (600 MHz) for a single residue undergoing two-site chemical exchange simulated with $T_{Ex} = 200$ ms, $p_E = 0.10$, $k_{ex} = 50\ s^{-1}$, $\Delta\varpi_{GE} = 5$ ppm, $B_1 = 25$ Hz with 10 % B_1 inhomogeneity (Vallurupalli et al. 2012), $R_1 = 0\ s^{-1}$ (**a**) and $R_1 = 2\ s^{-1}$ (**b**). *Red* and *blue* profiles were generated assuming 'non-equilibrium' and 'equilibrium' initial boundary conditions, respectively, and $R_{2,G} = R_{2,E} = 10\ s^{-1}$. The *insets in each panel* display the decay of ground state magnetization during T_{Ex} for the B_1 field applied at different ^{15}N offsets

Note that as R_1 increases ($R_1 = 0$ s^{-1} in a and 2 s^{-1} in b), the shift in the CEST baseline decreases and the size of the minor dip shrinks. For applications with very weak B_1 fields such that the rate of precession is slower than k_{ex}, small differences are, in fact, observed at the position of the minor state dip for different initial magnetization conditions, however, this effect is much less significant than the baseline shift (Figure S5).

Figure 3 establishes that, as with CPMG profiles, CEST curves also depend on initial magnetization conditions and because CEST data sets can be recorded with t_1 chemical shift evolution before (Vallurupalli et al. 2012) or after (Bouvignies et al. 2014) T_{Ex}, it is important that these conditions be taken into account correctly in the analysis of the relaxation data. In order to assess how sensitive CEST profiles are to initial boundary conditions and the resulting errors that are introduced to fitted parameters from using incorrect boundary values we have simulated ^{15}N CEST profiles for a range of k_{ex} and T_{Ex} values, 50 s^{-1} $\leq k_{ex} \leq$ 400 s^{-1}, 100 ms $\leq T_{Ex} \leq$ 450 ms. As in the CPMG analysis above, CEST data were generated with 'non-equilibrium' initial magnetization and then fit under the assumption of 'equilibrium' conditions, with the reverse situation considered in Supporting Information (Figure S6, Table S2). Simulations were performed for 21 residues using $\Delta\varpi_{GE}$ values that are the same as those experimentally determined for a K52C mutant of human telomerase factor 1, hTRF1, a small DNA binding protein (Sekhar et al. 2015). Data sets at two B_1 fields (15 Hz and 30 Hz) were constructed and the resulting CEST profiles fit globally to a two-site exchange model. The fitting parameters were then compared with input values to estimate the errors arising from use of the incorrect boundary conditions. As with CPMG, fitting errors are generally small, less than 10 %.

The magnitude of the relative fitting errors in CEST experiments obtained by using incorrect initial magnetization conditions can be estimated in a qualitative and intuitive manner, as for CPMG. The major CEST dip approaches zero in most cases due to saturation and most of the information about the exchange is thus inferred from the minor dip, whose height is approximately proportional to $k_{ex}T_{Ex}p_Ee^{-R_1T_{Ex}}$. Since the incorrect boundary condition causes a baseline shift of $\sim p_Ee^{-R_1T_{Ex}}$, as discussed above, effectively diminishing the size of the minor dip, the relative fitting error becomes proportional to the size of the baseline shift divided by the minor dip size, which is $1/(k_{ex}T_{Ex})$. Figure 4 shows the errors obtained from fitting data generated with the 'non-equilibrium' initial magnetization condition to a model that assumes 'equilibrium' initial magnetization, as a function of p_E, k_{ex}, and T_{Ex}. As for the CPMG case the 3D error surface is well characterized using the functional form $A/(k_{ex}T_{Ex})^c$, with c increasing slightly as R_1 deviates from 0 s^{-1}. Although fitting errors are small (<10 %) in most cases they do become relatively large as k_{ex} decreases to near the lower limit of the CEST experiment and T_{Ex} is short (e.g., $\sim$40 % fitting error in p_E for $k_{ex} = 50$ s^{-1} and $T_{Ex} = 100$ ms). Simulations were also performed using different ΔR_2 values (20 or 200 s^{-1}), with similar results to those obtained for $\Delta R_2 = 0$ s^{-1} (Table 2).

Examples from experimental CPMG and CEST data

Having established through simulation that relatively small errors in extracted exchange parameters are obtained by fitting data using incorrect initial boundary conditions we next analyzed experimental ^{15}N CPMG and ^{15}N CEST data sets to show that indeed this is the case. Experimental CPMG data sets were measured on L24A FF that has been characterized in detail previously (Korzhnev et al. 2010, 2011). We have analyzed the data assuming either 'equilibrium' or 'non-equilibrium' initial conditions (Fig. 5a). Since the dispersion profiles were recorded using a pulse scheme whereby the CPMG period precedes t_1 evolution (Vallurupalli et al. 2007), accurate exchange parameters should only be obtained from fits where 'equilibrium' initial magnetization values are used in the analysis (blue distribution of Fig. 5a). Relatively small differences in p_E and k_{ex} values are obtained from the fits (compare red and blue distributions), with errors on the order of 10 and 3 %, respectively. In a similar manner CEST data, recorded on the K52C mutant of hTRF1 that interconverts between a populated ground state and a sparse unfolded ensemble (Sekhar et al. 2015), were obtained using an experiment that places the CEST element prior to t_1 (Vallurupalli et al. 2012), so that the correct data analysis uses 'equilibrium' initial conditions. Very small (but quantifiable) errors are obtained when the data is analyzed incorrectly, as indicated in Fig. 5b. The errors in p_E and k_{ex} values observed in fits of the experimental data, that consist of residues covering a range of chemical exchange time-scales (Figure S7), are consistent with predictions based on simulations (see Supporting Information).

Dependence of amide ^{1}H $R_{1\rho}$ decay profiles on initial boundary conditions

In the previous sections we focused on the differences in CPMG and CEST relaxation profiles of ground state spins ($p_G \gg p_E$) that arise from varying the initial magnetization conditions. Here we explore how such initial conditions can influence relaxation profiles of excited state magnetization

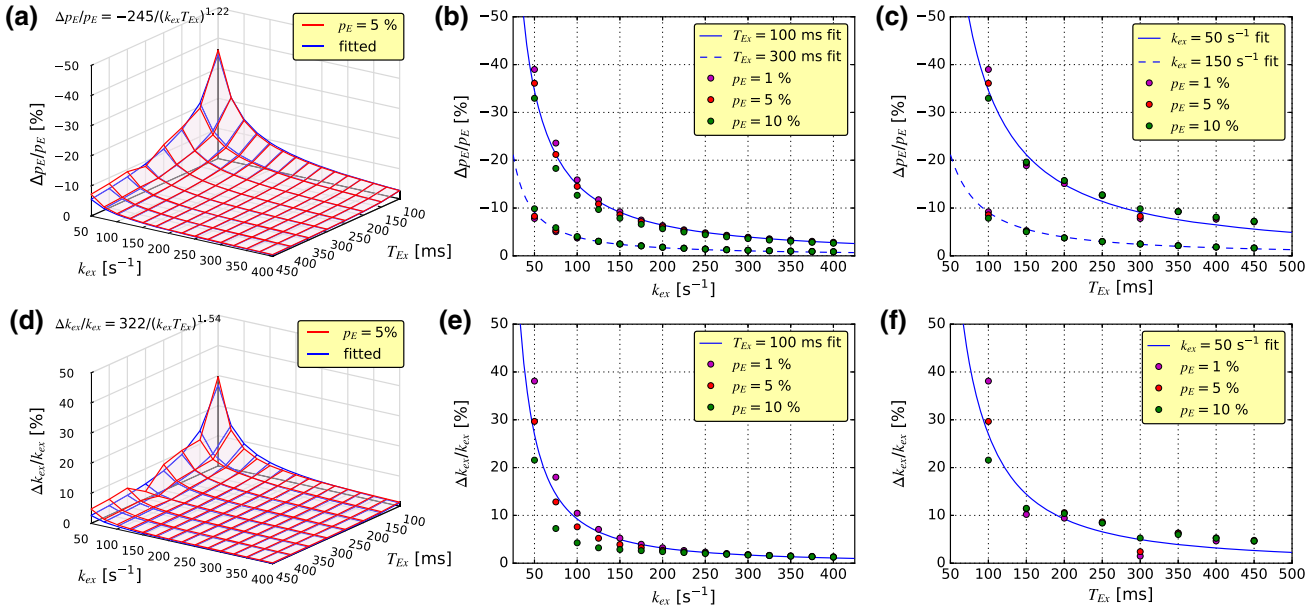

Fig. 4 Errors in exchange parameters derived from fitting ^{15}N CEST profiles generated using 'non-equilibrium' initial conditions and fit with equilibrium values of ground and excited state magnetization. **a**–**c** (**d**–**f**) Relative errors for fitted values of p_E (k_{ex}). **b**, **c** Two sets of simulated fitting errors for p_E with different T_{Ex} or k_{ex} values are displayed. A value of $R_1 = 2$ s^{-1} was assumed for both ground and excited state spins

Table 2 The pre-factor A and the exponential factor c, for the equation $A/(k_{ex}T_{Ex})^c$ describing the relative errors in fitting parameters when CEST profiles generated with 'non-equilibrium' boundary conditions are fit using equilibrium initial values of magnetization

	$R_1 = 0$ s^{-1}		$R_1 = 2$ s^{-1}		$R_1 = 4$ s^{-1}	
	A	c	A	c	A	c
p_E	−217	1.18	−245	1.22	−278	1.26
k_{ex}	192	1.35	322	1.54	576	1.77

The ground and excited state spins are assumed to have the same R_1 rate, indicated in the top horizontal line

that is monitored. We consider the case where protein (the 'excited' state) amide protons exchange with the surrounding reservoir of water (ground state) protons, with the detection of exchange carried out by monitoring the time dependence of protein magnetization in an $R_{1\rho}$ type of experiment (Ishima et al. 1998). In this example we have chosen an intrinsically disordered protein of 150 residues, 4E-BP2 (Bah et al. 2015), and measured amide ^{1}H $R_{1\rho}$ rates using three different experimental schemes illustrated schematically in Fig. 6, 30 °C, pH 6.5, where exchange of labile amide protons with water is expected to be substantial (Bai et al. 1993).

All 3 schemes are based on the HSQC pulse sequence, indicated schematically in Fig. 6, with amide ^{1}H $R_{1\rho}$ rates quantified by measuring the intensities of (^{15}N, ^{1}H) correlations in 2D spectra. In schemes 1 and 2 the ^{1}H spin-lock, denoted by the rectangular element of duration T_{relax}, is placed prior to t_1, while it is located immediately after the t_1 period in scheme 3. A relatively strong ^{1}H spin-lock field is employed ($\sim$6 kHz) so that in what follows we assume that the effective chemical shift difference between amide proton and water spins approaches zero ($\Delta\omega_{GE} \sim 0$). In scheme 1 the water magnetization is dephased initially by the application of a water selective pulse followed by a crusher gradient while water is preserved in the other two experiments through the application of selective pulses that restore solvent magnetization to the z-axis (Grzesiek and Bax 1993). The pulse schemes used are available from the authors upon request. Equations 1–5 (see above) are germane for the examples considered here with $p_E \ll 1$, however the inequality $\left|R_{1\rho,G} - R_{1\rho,E}\right| \ll k_{ex}$ need not hold presently. It follows, therefore, that $\lambda_1 \simeq -R_{1\rho,G}$, $\lambda_2 \simeq -R_{1\rho,E} - k_{ex}$ (Eq. 4).

In scheme 1 $M_{G,+}(0) = 0$ since water magnetization is fully eliminated and the decay of amide ^{1}H magnetization is described by

$$M_{E,+}(\tau) = \left[\begin{array}{l} \dfrac{p_E k_{ex}}{R_{1\rho,E} - R_{1\rho,G} + k_{ex}} e^{-R_{1\rho,G}\tau} \\ + \dfrac{R_{1\rho,E} - R_{1\rho,G} + (1-p_E)k_{ex}}{R_{1\rho,E} - R_{1\rho,G} + k_{ex}} e^{-(R_{1\rho,E}+k_{ex})\tau} \end{array}\right] M_{E,+}(0)$$
$$\simeq e^{-(R_{1\rho,E}+k_{ex})\tau} M_{E,+}(0). \quad (10)$$

The slowly decaying component (first term) can be neglected in this context since the magnitude of amide ^{1}H magnetization is much smaller than water ($p_E \sim 0.001$ %) (Yuwen and Skrynnikov 2014). Therefore the decay is

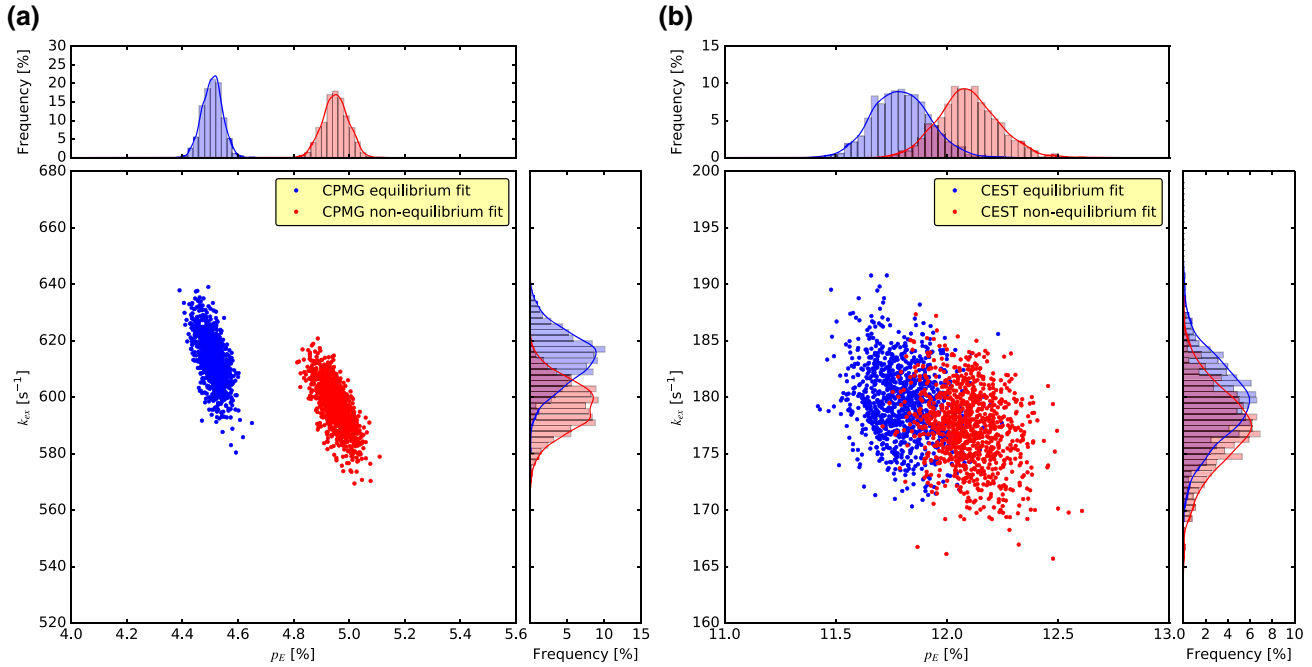

Fig. 5 Bootstrap analysis (Press et al. 1998) of experimental **a** ^{15}N CPMG relaxation dispersion data (L24A FF) and **b** ^{15}N CEST data (K52C hTRF1) with the number of bootstrap repeats N = 1000. Mean values of exchange parameters from analysis of CPMG data are $p_E = 4.5$ % and $k_{ex} = 614$ s^{-1}, fit under the (correct) assumption of 'equilibrium' boundary conditions and $p_E = 5.0$ %, $k_{ex} = 597$ s^{-1} when fit assuming 'non-equilibrium' boundary conditions. Mean values of exchange parameters are $p_E = 11.8$ % (12.1 %) and $k_{ex} = 180$ s^{-1} (177 s^{-1}) for CEST data fit with 'equilibrium' ('non-equilibrium) initial conditions. Since both experiments place T_{relax} or T_{Ex} before the t_1 evolution period and include equilibration elements before and after T_{relax}/T_{Ex} (Hansen et al. 2008) data analysis using 'equilibrium' initial boundary condition is correct

essentially mono-exponential. By contrast, in scheme 2 the system is at equilibrium at the beginning of the ^{1}H spin-lock so that $k_{GE}M_{G,+}(0) = k_{EG}M_{E,+}(0)$, and the amide ^{1}H magnetization decay is bi-exponential

$$M_{E,+}(\tau) = \left[\begin{array}{l} \dfrac{k_{ex}}{R_{1\rho,E} - R_{1\rho,G} + k_{ex}} e^{-R_{1\rho,G}\tau} \\ + \dfrac{R_{1\rho,E} - R_{1\rho,G}}{R_{1\rho,E} - R_{1\rho,G} + k_{ex}} e^{-(R_{1\rho,E}+k_{ex})\tau} \end{array} \right] M_{E,+}(0). \quad (11)$$

In practice, since the transverse water magnetization relaxes much more slowly than transverse amide ^{1}H magnetization ($R_{1\rho,G} \ll R_{1\rho,E}$), the slowly decaying component (first term) can be treated as a constant during the short ^{1}H spin-lock interval so that the evolution of amide ^{1}H magnetization can be described by a modified mono-exponential decay function of the form $Ae^{-R\tau} + C$ (Fig. 6). Finally, scheme 3 measures the decay of anti-phase amide proton magnetization. In this case magnetization decay profiles are expected to be similar to those generated from scheme 1 since in both cases the effective initial boundary condition for water is $M_{G,+}(0) = 0$, leading to an increase in the apparent relaxation rates of amide proton spins by k_{ex}. However, rates measured from schemes 1 and 3 are not expected to be identical since, as described by Ishima et al., placement of the ^{1}H spin-lock element after t_1, eliminates contributions to $R_{1\rho}$ from ^{1}H–^{1}H dipolar cross-relaxation (Ishima et al. 1998), such that decay rates measured from scheme 3 are expected to be lower than those obtained with scheme 1. For example, $R_{1\rho}$ rates for schemes 1 and 3 are given by

$$\begin{aligned} R_{1\rho,\text{like}} &= \frac{9}{20}\frac{\gamma_H^4\hbar^2}{r_{HH}^6}S^2\tau_c \quad \text{(scheme 1)}, \\ R_{1\rho,\text{unlike}} &= \frac{1}{4}\frac{\gamma_H^4\hbar^2}{r_{HH}^6}S^2\tau_c \quad \text{(scheme 3)} \end{aligned} \quad (12)$$

with predicted differences on the order of ~ 15 s^{-1} for a protein tumbling isotropically with a correlation time (τ_c) of 5 ns, assuming an order parameter $S^2 = 1$ and an effective ^{1}H–^{1}H distance (r_{HH}) of 1.82 Å, as would be expected for a fully protonated sample.

Figure 6 shows decay profiles measured for a pair of amide ^{1}H spins in 4E-BP2. The pronounced biexponential decay of transverse magnetization obtained via scheme 2 is obvious, as is the mono-exponential decay of magnetization recorded via schemes 1 and 3. Differences are observed experimentally between schemes 1 and 3, as expected, where $R_{1\rho}$ rates

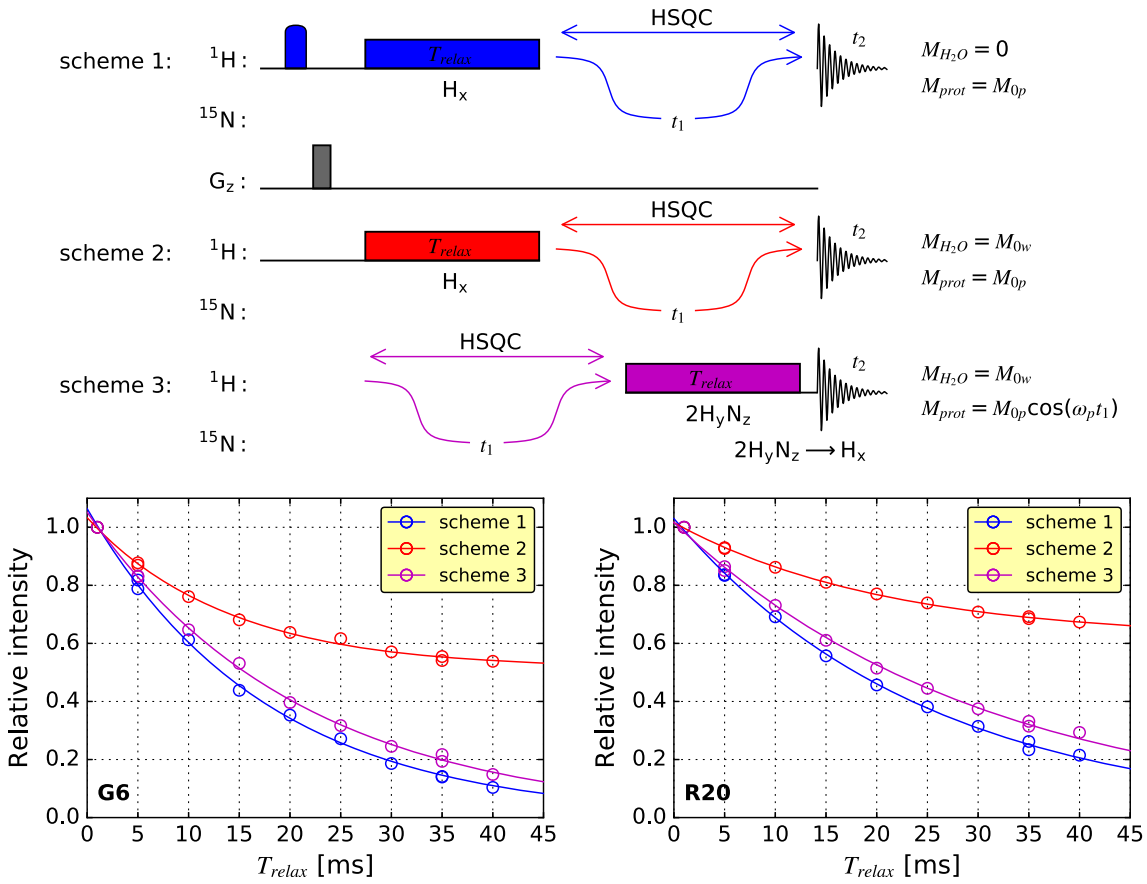

Fig. 6 ^{1}H intensity decay profiles measured in $R_{1\rho}$ experiments (scheme 1–3) depend on initial boundary conditions. Schemes 1 and 2 place the ^{1}H spin lock (represented by the *long rectangles*) before the ^{15}N chemical shift labeling period (t_1), while scheme 3 places the spin lock after t_1. Scheme 1 applies an additional 90° selective pulse on water (indicated by the *blue half rounded rectangle*) before a purge gradient (represented by the *grey rectangle*) to fully eliminate water magnetization prior to T_{relax}. The decay profiles for residues G6 and R20 of the intrinsically disordered protein 4E-BP2 obtained with schemes 1–3 are illustrated. Profiles from schemes 1 and 3 decay in a mono-exponential manner, while decay profiles from scheme 2 are more complex due to solvent exchange

measured with scheme 1 are, on average, 6 s^{-1} larger than those measured with scheme 3 (Figure S8). It is clear that initial boundary conditions are critical in this class of experiment and that the differences are much more pronounced when the sparsely populated state is detected than when the ground state is observed.

Conclusions

In the past several years a number of different spin relaxation experiments have been developed for probing conformationally excited states of biomolecules in solution. Central have been CPMG- and CEST-based schemes for the measurement of ms (or slower) chemical exchange processes that are often of great relevance for biological function. Given the potential of these experiments and their growing popularity it is important that data analyses be carried out as rigorously as possible, taking into account experimental details that often vary from one implementation to the next. Here we have examined how initial boundary conditions can influence both CPMG and CEST profiles and, importantly, the resulting errors that occur when incorrect initial magnetization conditions are used in data analysis. This is particularly relevant since the majority of analyses assume equilibrium values of ground and excited state magnetization at the start of CPMG/CEST relaxation elements and this assumption is not necessarily correct. In general, it is advisable to take boundary conditions into account in all analyses of CPMG/CEST data without a priori (and potentially incorrect) assumptions. In the case where the relaxation elements precede t_1 it is reasonable to assume that the initial magnetization values are simply those present at equilibrium. This is, however, complicated by the fact that magnetization from spins in ground and excited states will decay differently during magnetization transfer elements, in general, and it is becomes difficult, therefore, to accurately obtain correct estimates for the initial conditions. We recommend,

therefore, placement of equilibration periods prior to the CPMG/CEST relaxation elements, recognizing that for systems in relatively slow exchange full equilibration is unlikely to occur. The 'cleanest' experimental approach is to place t_1 prior to CPMG/CEST delays as then the boundary conditions are well approximated by (p_G, 0) for the ground and excited state components, respectively, so long as chemical shifts of spins in each state are non-degenerate. While correct boundary conditions can thus be obtained, independent of differential relaxation of spins in the interconverting states, it is not possible to preserve both coherence pathways using this approach and thus experimental sensitivity is reduced by as much as 40 %. Fortunately, as we have shown, errors in the resulting fitting parameters from using incorrect boundary conditions are, in general, small and typically less than 10 % of the actual value. As k_{ex} decreases to values that are at the low end for CPMG or CEST experiments, 400 and 50 s^{-1}, respectively, fractional errors can increase to 20–40 % and analyses, especially in these cases, must be carried out with more care.

Acknowledgments We thank Enrico Rennella for helpful discussions and Rina Rosenzweig, Alaji Bah and Jacob Brady for providing protein samples. This project is supported by grants from the Canadian Institutes of Health Research and the Natural Sciences and Engineering Research Council of Canada. L.E.K. holds a Canada Research Chair in Biochemistry.

References

Bah A et al (2015) Folding of an intrinsically disordered protein by phosphorylation as a regulatory switch. Nature 519:106-U240. doi:10.1038/nature13999

Bai YW, Milne JS, Mayne L, Englander SW (1993) Primary structure effects on peptide group hydrogen exchange. Proteins 17:75–86. doi:10.1002/prot.340170110

Baldwin AJ, Kay LE (2009) NMR spectroscopy brings invisible protein states into focus. Nat Chem Biol 5:808–814. doi:10.1038/nchembio.238

Baldwin AJ, Kay LE (2013) An $R_{1\rho}$ expression for a spin in chemical exchange between two sites with unequal transverse relaxation rates. J Biomol NMR 55:211–218. doi:10.1007/s10858-012-9694-6

Boehr DD, McElheny D, Dyson HJ, Wright PE (2006) The dynamic energy landscape of dihydrofolate reductase catalysis. Science 313:1638–1642. doi:10.1126/science.1130258

Bouvignies G, Vallurupalli P, Kay LE (2014) Visualizing side chains of invisible protein conformers by solution NMR. J Mol Biol 426:763–774. doi:10.1016/j.jmb.2013.10.041

Farrow NA, Zhang OW, Forman-Kay JD, Kay LE (1994) A heteronuclear correlation experiment for simultaneous determination of ^{15}N longitudinal decay and chemical exchange rates of systems in slow equilibrium. J Biomol NMR 4:727–734. doi:10.1007/Bf00404280

Fawzi NL, Ying JF, Ghirlando R, Torchia DA, Clore GM (2011) Atomic-resolution dynamics on the surface of amyloid-beta protofibrils probed by solution NMR. Nature 480:268-U161. doi:10.1038/nature10577

Grzesiek S, Bax A (1993) The importance of not saturating H_2O in protein NMR. Application to sensitivity enhancement and NOE measurements. J Am Chem Soc 115:12593–12594. doi:10.1021/ja00079a052

Hansen DF, Led JJ (2003) Implications of using approximate Bloch–McConnell equations in NMR analyses of chemically exchanging systems: application to the electron self-exchange of plastocyanin. J Magn Reson 163:215–227. doi:10.1016/S1090-7807(03)00062-4

Hansen DF, Vallurupalli P, Lundstrom P, Neudecker P, Kay LE (2008) Probing chemical shifts of invisible states of proteins with relaxation dispersion NMR spectroscopy: how well can we do? J Am Chem Soc 130:2667–2675. doi:10.1021/ja078337p

Hansen AL, Lundstrom P, Velyvis A, Kay LE (2012) Quantifying millisecond exchange dynamics in proteins by CPMG relaxation dispersion NMR using side-chain ^{1}H probes. J Am Chem Soc 134:3178–3189. doi:10.1021/ja210711v

Henzler-Wildman KA et al (2007) Intrinsic motions along an enzymatic reaction trajectory. Nature 450:838-U813. doi:10.1038/nature06410

Ishima R, Torchia DA (2003) Extending the range of amide proton relaxation dispersion experiments in proteins using a constant-time relaxation-compensated CPMG approach. J Biomol NMR 25:243–248. doi:10.1023/A:1022851228405

Ishima R, Torchia DA (2005) Error estimation and global fitting in transverse-relaxation dispersion experiments to determine chemical-exchange parameters. J Biomol NMR 32:41–54. doi:10.1007/s10858-005-3593-z

Ishima R, Torchia DA (2006) Accuracy of optimized chemical-exchange parameters derived by fitting CPMG R_2 dispersion profiles when $R_2^{0a} \neq R_2^{0b}$. J Biomol NMR 34:209–219. doi:10.1007/s10858-005-6226-7

Ishima R, Wingfield PT, Stahl SJ, Kaufman JD, Torchia DA (1998) Using amide ^{1}H and ^{15}N transverse relaxation to detect millisecond time-scale motions in perdeuterated proteins: application to HIV-1 protease. J Am Chem Soc 120:10534–10542. doi:10.1021/ja981546c

Ishima R, Louis JM, Torchia DA (1999) Transverse ^{1}H cross relaxation in ^{1}H–^{15}N correlated ^{1}H CPMG experiments. J Magn Reson 137:289–292. doi:10.1006/jmre.1998.1672

Ishima R, Louis JM, Torchia DA (2001) Characterization of two hydrophobic methyl clusters in HIV-1 protease by NMR spin relaxation in solution. J Mol Biol 305:515–521. doi:10.1006/jmbi.2000.4321

Karplus M, Kuriyan J (2005) Molecular dynamics and protein function. Proc Natl Acad Sci USA 102:6679–6685. doi:10.1073/pnas.0408930102

Kay LE, Keifer P, Saarinen T (1992) Pure absorption gradient enhanced heteronuclear single quantum correlation spectroscopy with improved sensitivity. J Am Chem Soc 114:10663–10665. doi:10.1021/ja00052a088

Korzhnev DM, Salvatella X, Vendruscolo M, Di Nardo AA, Davidson AR, Dobson CM, Kay LE (2004) Low-populated folding intermediates of Fyn SH3 characterized by relaxation dispersion NMR. Nature 430:586–590. doi:10.1038/nature02655

Korzhnev DM, Bezsonova I, Lee S, Chalikian TV, Kay LE (2009) Alternate binding modes for a ubiquitin-SH3 domain interaction studied by NMR spectroscopy. J Mol Biol 386:391–405. doi:10.1016/j.jmb.2008.11.055

Korzhnev DM, Religa TL, Banachewicz W, Fersht AR, Kay LE (2010) A transient and low-populated protein-folding intermediate at atomic resolution. Science 329:1312–1316. doi:10.1126/science.1191723

Korzhnev DM, Vernon RM, Religa TL, Hansen AL, Baker D, Fersht AR, Kay LE (2011) Nonnative interactions in the FF domain folding pathway from an atomic resolution structure of a sparsely populated intermediate: an NMR relaxation dispersion study. J Am Chem Soc 133:10974–10982. doi:10.1021/ja203686t

Kovrigin EL, Kempf JG, Grey MJ, Loria JP (2006) Faithful estimation of dynamics parameters from CPMG relaxation dispersion measurements. J Magn Reson 180:93–104. doi:10.1016/j.jmr.2006.01.010

Lukhele S, Bah A, Lin H, Sonenberg N, Forman-Kay JD (2013) Interaction of the eukaryotic initiation factor 4E with 4E-BP2 at a dynamic bipartite interface. Structure 21:2186–2196. doi:10.1016/j.str.2013.08.030

Mangia S, Traaseth NJ, Veglia G, Garwood M, Michaeli S (2010) Probing slow protein dynamics by adiabatic $R_{1\rho}$ and $R_{2\rho}$ NMR experiments. J Am Chem Soc 132:9979–9981. doi:10.1021/ja1038787

McConnell HM (1958) Reaction rates by nuclear magnetic resonance. J Chem Phys 28:430–431. doi:10.1063/1.1744152

Mittermaier AK, Kay LE (2006) New tools provide new insights in NMR studies of protein dynamics. Science 312:224–228. doi:10.1126/science.1124964

Mittermaier AK, Kay LE (2009) Observing biological dynamics at atomic resolution using NMR. Trends Biochem Sci 34:601–611. doi:10.1016/j.tibs.2009.07.004

Montelione GT, Wagner G (1989) 2D chemical exchange NMR spectroscopy by proton-detected heteronuclear correlation. J Am Chem Soc 111:3096–3098. doi:10.1021/ja00190a072

Mulder FAA, Skrynnikov NR, Hon B, Dahlquist FW, Kay LE (2001) Measurement of slow (μs–ms) time scale dynamics in protein side chains by ^{15}N relaxation dispersion NMR spectroscopy: application to Asn and Gln residues in a cavity mutant of T4 lysozyme. J Am Chem Soc 123:967–975. doi:10.1021/ja003447g

Neudecker P et al (2012) Structure of an intermediate state in protein folding and aggregation. Science 336:362–366. doi:10.1126/science.1214203

Noggle JH, Schirmer RE (1971) The nuclear Overhauser effect. Academic Press, London

Palmer AG (2014) Chemical exchange in biomacromolecules: past, present, and future. J Magn Reson 241:3–17. doi:10.1016/j.jmr.2014.01.008

Palmer AG (2015) Enzyme dynamics from NMR spectroscopy. Acc Chem Res 48:457–465. doi:10.1021/ar500340a

Palmer AG, Massi F (2006) Characterization of the dynamics of biomacromolecules using rotating-frame spin relaxation NMR spectroscopy. Chem Rev 106:1700–1719. doi:10.1021/cr0404287

Palmer AG, Cavanagh J, Wright PE, Rance M (1991) Sensitivity improvement in proton-detected two-dimensional heteronuclear correlation NMR spectroscopy. J Magn Reson 93:151–170. doi:10.1016/0022-2364(91)90036-S

Palmer AG, Kroenke CD, Loria JP (2001) Nuclear magnetic resonance methods for quantifying microsecond-to-millisecond motions in biological macromolecules. Methods Enzymol 339:204–238. doi:10.1016/S0076-6879(01)39315-1

Press WH, Teukolsky SA, Vetterling WT, Flannery BP (1998) Numerical recipes in C, 2nd edn. Cambridge University Press, Cambridge

Rivalta I, Sultan MM, Lee NS, Manley GA, Loria JP, Batista VS (2012) Allosteric pathways in imidazole glycerol phosphate synthase. Proc Natl Acad Sci USA 109:E1428–E1436. doi:10.1073/pnas.1120536109

Schleucher J, Sattler M, Griesinger C (1993) Coherence selection by gradients without signal attenuation: application to the three-dimensional HNCO experiment. Angew Chem Int Ed 32:1489–1491. doi:10.1002/anie.199314891

Sekhar A, Kay LE (2013) NMR paves the way for atomic level descriptions of sparsely populated, transiently formed biomolecular conformers. Proc Natl Acad Sci USA 110:12867–12874. doi:10.1073/pnas.1305688110

Sekhar A, Rosenzweig R, Bouvignies G, Kay LE (2015) Mapping the conformation of a client protein through the Hsp70 functional cycle. Proc Natl Acad Sci USA 112:10395–10400. doi:10.1073/pnas.1508504112

Sklenar V, Torchia D, Bax A (1987) Measurement of ^{13}C longitudinal relaxation using ^{1}H detection. J Magn Reson 73:375–379. doi:10.1016/0022-2364(87)90214-9

Sugase K, Dyson HJ, Wright PE (2007) Mechanism of coupled folding and binding of an intrinsically disordered protein. Nature 447:1021-U1011. doi:10.1038/nature05858

Traaseth NJ et al (2012) Heteronuclear Adiabatic Relaxation Dispersion (HARD) for quantitative analysis of conformational dynamics in proteins. J Magn Reson 219:75–82. doi:10.1016/j.jmr.2012.03.024

Vallurupalli P, Hansen DF, Stollar E, Meirovitch E, Kay LE (2007) Measurement of bond vector orientations in invisible excited states of proteins. Proc Natl Acad Sci USA 104:18473–18477. doi:10.1073/pnas.0708296104

Vallurupalli P, Bouvignies G, Kay LE (2012) Studying "invisible" excited protein states in slow exchange with a major state conformation. J Am Chem Soc 134:8148–8161. doi:10.1021/ja3001419

Wang CY, Rance M, Palmer AG (2003) Mapping chemical exchange in proteins with MW > 50 kD. J Am Chem Soc 125:8968–8969. doi:10.1021/ja035139z

Yuwen T, Skrynnikov NR (2014) CP-HISQC: a better version of HSQC experiment for intrinsically disordered proteins under physiological conditions. J Biomol NMR 58:175–192. doi:10.1007/s10858-014-9815-5